

Fermi Nesting between Atomic Wires with Strong Spin-Orbit Coupling

C. Tegenkamp,^{1,*} D. Lükermann,¹ H. Pfürer,¹ B. Slomski,^{2,3} G. Landolt,^{2,3} and J. H. Dil^{2,3}

¹*Institut für Festkörperphysik, Leibniz Universität Hannover, Appelstraße 2, 30167 Hannover, Germany*

²*Physik-Institut, Universität Zürich, Winterthurerstrasse 190, 8057 Zürich, Switzerland*

³*Swiss Light Source, Paul Scherrer Institut, 5232 Villigen PSI, Switzerland*

(Received 3 August 2012; published 26 December 2012)

The mutual interplay between superlattice structures, band filling factors, and spin-orbit coupling results in a highly correlated electronic spin and charge state found for an array of atomic Pb wires grown on Si(557). By means of spin- and angle-resolved photoemission spectroscopy, the spin texture close to the Fermi surface was found to be alternating and equidistant; thus, Fermi nesting occurs in between bands with the same spin helicity, giving rise to spin-polarized charge-density waves in the direction across the wires. An out-of-phase superposition of both Rashba channels is manifested by an extraordinary large Rashba splitting of $\Delta k_0 = 0.2 \text{ \AA}^{-1} = g/2$, where g is a reciprocal lattice vector defined by the interwire distance and fits into the model of spin-density waves in antiferromagnetically ordered chain structures. The implications towards spin-polarized transport along the wires will be discussed.

DOI: [10.1103/PhysRevLett.109.266401](https://doi.org/10.1103/PhysRevLett.109.266401)

PACS numbers: 71.45.Lr, 75.30.Fv

The intriguing physics of quasi-one-dimensional (1D) systems [1] can be successfully realized with atomic wires grown by self-assembly on surfaces [2,3]. The controlled embedding of these structures onto or into the surface opens the pathway for studying exotic phenomena such as charge-density waves and Luttinger liquid behavior in metallic nanostructures [4]. However, the role of spin-orbit coupling (SOC) in these electronically correlated systems is hardly explored and came only lately in the focus of research.

As a consequence of the broken inversion symmetry, SOC leads inevitably to spin-polarized states in these low-dimensional systems at surfaces [5]. In the case of Au/Si(553), the ground state reveals an intrinsic magnetism at the surface [6]. The size of the Rashba splitting depends on the intra-atomic spin-orbit coupling (high- Z materials), on the surface potential gradient dV/dz , and on the charge distribution $\rho(r)$ [7–9]. Consequently, the surface structure as well as hybridization between orbitals with different parities are important and strongly influence the splitting of the states [10]. The effect is parametrized by the Rashba constant $\alpha_R = \Delta k_0 \hbar^2 / 2m^*$, where \hbar denotes the reduced Planck constant, m^* the effective mass, and $\Delta k_0 = 2k_0$ the momentum splitting of the spin-polarized bands.

In quasi-1D array structures, the coupling strengths of the wires within the ensemble and the substrate are decisive. As shown, e.g., for Au submonolayers adsorbed on vicinal Si(111) surfaces [11], dispersing electronic states are found only in the direction along the wires. Alternatively, superlattice structures can be used in order to trigger 1D properties, e.g., as seen for Pb/Si(557). For this system, strong coupling of adjacent wires has revealed 1D transport due to Fermi nesting in the direction across the wires; however, the role of SOC in this system has not been taken into account so far [12,13].

An interesting question arises now of how the surface band structure is modified and correlation effects are affected if both strong SOC and superlattice structures coexist. As sketched in Fig. 1, different spin-texture scenarios are expected at the Fermi surface (FS), in particular, if the band filling is also taken into account. For Au wires on vicinal Si(111), indeed, SO-split surface bands have been found (only) along the wire direction. The splitting of $\Delta k_0 = 0.05 \text{ \AA}^{-1}$ found for this system is comparably small [14,15]. The question has been addressed as well to vicinal Au(111), the prototype system for lateral quantum well effects. While in the case of low step densities the spin-split surface state and umklapp states incoherently overlap, only for highly stepped surfaces, e.g., Au(223), has a small enhancement of the SOC been found [16]. However, implications toward collective phenomena like magnetic ordering, etc., are not in the focus of research yet.

In this Letter, we show that for 1.3 ML Pb/Si(557) the interplay between superlattice structure, chemical potential, and Rashba splitting leads to a highly correlated electronic state. SOC results in spin-polarized metallic surface bands along the wires in agreement with recently performed magnetotransport measurements [17]. For the direction across the wires, simultaneous Fermi nesting is found for both Rashba channels ($|2k_{\Gamma(1)}| = g$), suggesting the formation of two spin-polarized charge-density waves (CDW). Furthermore, the extraordinary large Rashba splitting of $g/2$ can be explained reasonably by formation of a spin-density wave (SDW), which is the ground state of CDWs with strong electron-electron interaction [18]. The Pb/Si(557) system nicely demonstrates the close relation between charge- and spin-density waves in the presence of SOC and electron-correlation effects.

Spin- and angle-resolved photoemission [(S)ARPES] measurements have been performed at the COPHEE end

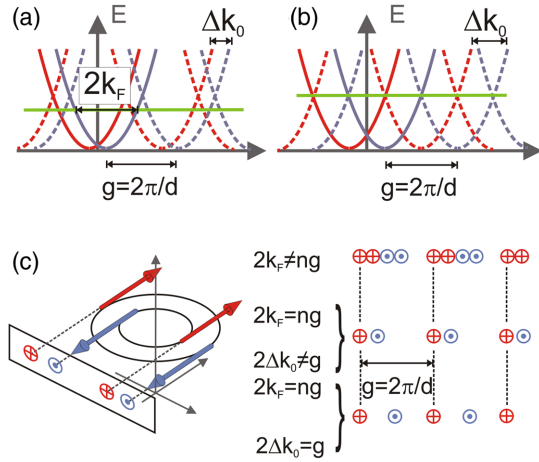


FIG. 1 (color online). Illustration of the interplay between the chemical potential and superlattice symmetry in a surface system with SOC, parametrized by k_F , $g = 2\pi/d$, and Δk_0 , respectively. (a) and (b) represent two extreme cases, where k_F and Δk_0 are completely incommensurate and commensurate, respectively, for a given umklapp sequence g . (c) Only if both conditions $2k_{F,i} = ng$ (n , integer; $i = \uparrow, \downarrow$) and $2\Delta k_0 = g$ are fulfilled does the spin texture at E_F appear alternating and equidistant in a spin-resolved ARPES experiment.

station at the SIS beamline at the Swiss Light Source [19]. The wires were grown *in situ* by evaporation of Pb on Si (557) substrates. The morphology of the clean Si(557) substrate, obtained after several cycles of flashing, as well as the structure of the wire ensemble, has been checked by LEED [cf. Fig. 2(a)]. Details about the preparation and coverage calibration are reported elsewhere [13]. The photoemission experiments were performed with p -polarized light (mostly $h\nu = 24$ eV) at 60 K at a base pressure of 1×10^{-8} Pa. By recording intensities and spin-induced scattering asymmetries with the two orthogonal Mott detectors for different emission angles, spin-resolved momentum distribution curves (MDCs) close to the Fermi energy have been measured. In order to reveal good signal-to-noise ratios in reasonable time, the spin distribution has been measured 100 meV below the Fermi surface.

Upon adsorption of Pb at 640 K, the Si(557) surface undergoes refacetting [20,21]. For a coverage of 1.3 ML, the small (111) terraces of $4\frac{2}{3}$ atomic units in the width of the (223) facet structure are occupied by Pb atoms, as sketched in Fig. 2(b). The structure of this particular superlattice shows up as replicas in photoemission. As is obvious from the constant energy surface taken at $E_F - 100$ meV [Fig. 2(c)] and the momentum distribution curve shown in Fig. 2(e), the reciprocal lattice vector $g = 2\pi/d = 0.4 \text{ \AA}^{-1}$ is defined by the interwire distance $d = 1.58$ nm, in agreement with former studies [13,22]. Qualitatively, the complex contour close to E_F can be explained by replicas of circles, which reflects the local 2D character of the densely packed $\alpha\sqrt{3} \times \sqrt{3}$ phase

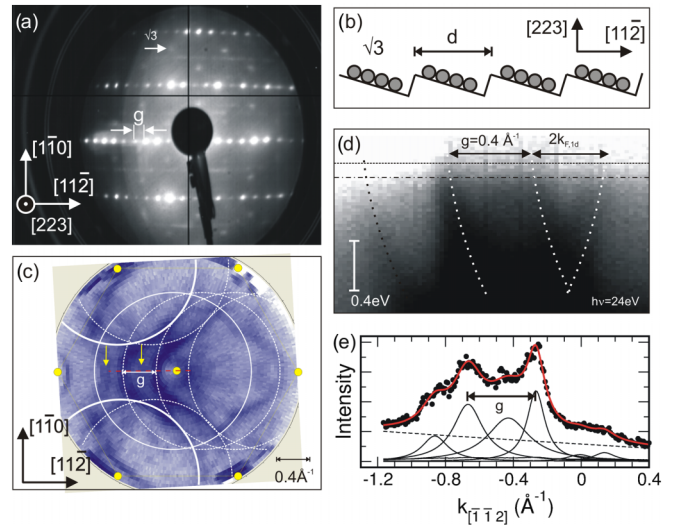


FIG. 2 (color online). (a) LEED image of 1.31 ML Pb adsorbed on Si(557). The equidistant spot splitting of $g = 2\pi/d$ along the $[11\bar{2}]$ direction is indicative for a long range ordered (223) facet with an average step separation d as sketched schematically in (b). The constant energy surface shown in (c), taken at $E_F - 100$ meV, can be explained by circles (of one spin polarization) around the Γ points (yellow points) as well as the umklapp states (dashed lines). For better visibility, only a few are drawn. (d) $E(k)$ diagram along the $[11\bar{2}]$ direction at $k_{[1\bar{1}0]} = 0 \text{ \AA}^{-1}$. The momentum distribution curves were taken at $E_F - 100$ meV (dash-dotted line). (e) The MDC taken along the dashed line in (c) shows, besides the primary umklapp structure (g periodicity), also a substructure shifted by around 0.2 \AA^{-1} . The data shown were measured with the spin-integrating detector. For further details, see the text.

of Pb on the mini-(111) terraces [cf. Fig. 2(b)]. One of the peculiar properties and robust signatures of this phase is that, along the $[11\bar{2}]$ direction, the band filling of the surface states is such that $2k_F = g$ [Fig. 2(d)]. This nesting condition leads to a renormalization of the circles close to E_F ; i.e., the curvature of the circles flattens, as close inspection of the constant energy plots shown in Figs. 2(c) and 5(b) suggests. For reasons of simplicity, the renormalization effect is not considered in the schematics shown. In our former study, we have shown further that this perfect Fermi nesting in the direction across the wires is accompanied with the formation of small band gaps in the order of 20 meV at E_F . Details can be found in Ref. [13].

Besides the intense umklapp structure, the constant energy map (see arrows in Fig. 2(c)) as well as the spin-integrated MDC, both taken 100 meV below E_F , reveal a substructure that is less in intensity and shifted by around 0.2 \AA^{-1} with respect to the dominant replica structure. As we will see in the following, the substructure originates from SOC in this system.

In order to elucidate the spin texture of the electronic bands close to the Fermi surface, SARPES spectra were

taken along different crystallographic directions. In this study, we will restrict ourselves to the $[11\bar{2}]$ direction, where the analysis of the spin-resolved data is not limited by resolution. It is quite obvious from the reassembly by circles of the constant energy plot close to E_F , as shown for a few in Fig. 2(c), that in other regions of the surface Brillouin zone many bands intersect, increasing the complexity, especially if spin-split surface states are taken into account.

Figure 3(a) shows a characteristic MDC curve measured with the Mott detectors along the $[11\bar{2}]$ direction at $k_x = k_{[110]} = 0 \text{ \AA}^{-1}$, i.e., the direction at which perfect nesting occurs for the 1.3 ML phase [cf. Fig. 2(d)]. In agreement with the findings, in the context of Fig. 2(e), an almost perfect modeling of the intensity distribution is possible by pseudo-Voigt peaks separated by 0.2 \AA^{-1} , i.e., half of the reciprocal lattice vector. The corresponding spin asymmetries measured with the Mott detectors and weighted with the system-specific Sherman function are shown in Fig. 3(b) for (P_x, P_y, P_z) . A spin polarization of around 40% is measured for the component perpendicular to the direction of the momentum, i.e., along the $[1\bar{1}0]$ direction for P_x , while the y and z components do not show a clear polarization signal. Following the procedures for the data analysis described in detail in Refs. [23,24], the main features of the total intensity and polarization can be reasonably reproduced if the spin vector of all surface bands has only in-plane components and if the x component shows an alternating orientation. Hereby, it is assumed that the bands are fully spin polarized. The resulting components of the spin polarization vector are depicted in Fig. 3(a) for the single MDC peaks.

The spin analysis for the 1.3 ML phase reveals several interesting findings: The spin polarization of the

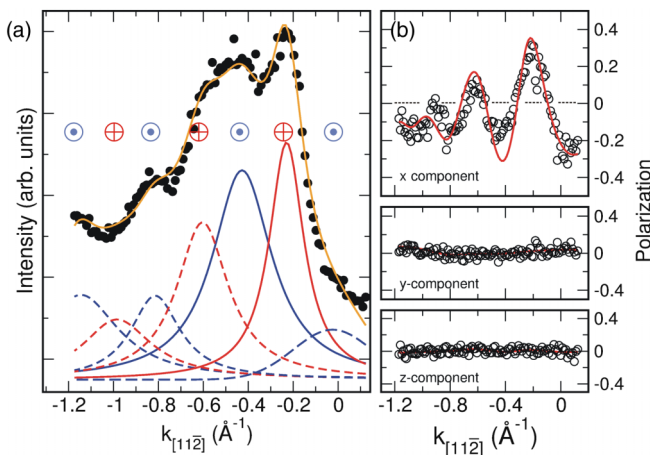


FIG. 3 (color online). (a) MDC measured at $E_F - 100 \text{ meV}$ with the Mott detectors for 1.3 ML Pb on Si(557). (b) Spin polarizations measured with the Mott detectors for each spatial component. The pronounced polarization along the $[11\bar{2}]$ direction for the x component is indicated by \oplus and \ominus in (a).

electrons is perpendicular to the direction of motion and the surface potential gradient, as expected for a free 2D electron gas and in accordance with our assembly model of the FS by circles [cf. Fig. 2(c)]. Second, the spin polarization is alternating close to (at) the FS, and, most importantly, the Fermi nesting is maintained between surface bands with the same spin helicity. As mentioned above, this finding is an expected signature for a system where the chemical potential coincides with the crossing points defined by replica structures. Finally, the Rashba splitting $\Delta k_0 = 0.2 \text{ \AA}^{-1}$ found along the k_y direction is extremely large and, interestingly, half the size of the reciprocal lattice vector g ; i.e., it takes its maximum value. A qualitative discussion about its magnitude is given below. Nonetheless, the oscillatory behavior of P_x demands unambiguously an alternating spin texture at the FS.

In order to prove this model further, a spin analysis for a Pb/Si(557) with a coverage of 1.2 ML has been performed. For this coverage, it is known that the long range ordered (223) facet structure is preserved but with a lower Pb concentration [20]; i.e., the chemical potential is different than that of the 1.3 ML case. In LEED [cf. Fig. 4(c)], the spot splitting is the same as for the 1.3 ML phase [cf. Fig. 2(a)] but $\sqrt{3}$ superstructure spots are missing. Accordingly, replica structures with $g = 0.4 \text{ \AA}^{-1}$ are seen in ARPES; however, the nesting condition is not fulfilled, as is obvious from the energy dispersion shown in Fig. 4(b).

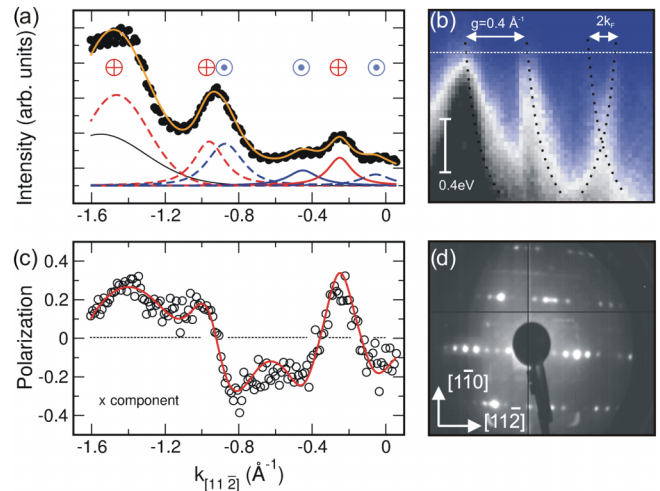


FIG. 4 (color online). (a) MDC measured at $E_F - 100 \text{ meV}$ with the Mott detectors for 1.2 ML Pb. (b) $E(k)$ diagram in order to show the imperfect Fermi nesting condition ($2k_f \neq g$; the dashed lines are guides to the eyes). (c) Spin polarization measured with the Mott detectors. The projected spin components are shown accordingly by \oplus and \ominus in (a). The ARPES measurements were performed with $h\nu = 44 \text{ eV}$. (d) LEED pattern of the 1.2 ML phase; the $\sqrt{3}$ superstructure spots are missing.

Compared to the 1.3 ML phase, the spin texture of the 1.2 ML phase behaves completely differently. The MDC and corresponding spin polarization for the x component are shown in Figs. 4(a) and 4(c), respectively. As in the case of 1.3 ML, the bands are again fully polarized and the spin polarization vector lies within the surface plane and perpendicular to the direction of the electron motion; however, the spin texture is not oscillating with a period of 0.2 \AA^{-1} in accordance with the simple model presented in the context of Fig. 1. The difference of the spin textures present in the 1.3 and 1.2 ML cases is directly evident by comparison of Figs. 3(b) and 4(c) respectively. To be more specific, the intensity distribution and the spin polarizations can be modeled only if the spins are assumed to be nonalternatingly arranged. The Rashba splitting for 1.2 ML is found to be the same as for 1.3 ML; thus, within the experimental resolution, α_R is not affected by a different chemical potential.

The SARPES measurements have revealed the presence of a strongly spin-polarized Fermi surface, as shown in Fig. 5, which has interesting implications toward electronic transport and, particularly, magnetotransport measurements that can probe SOC if weak localization is present in the system [17]. Although the spin-resolved data were taken 100 meV below E_F it should be permitted to assume that the spin texture is maintained at the FS. For the 1.3 ML phase at temperatures below 80 K, nesting in the direction across the wires ($[11\bar{2}]$ direction) occurs between surface bands of the same helicity. As a consequence, metallic conductivity was found only along the wires ($[1\bar{1}0]$ direction) with a strong suppression of spin-orbit scattering in these states [17]. Furthermore, because of the spin texture of the FS, an injected spin will precess when transported along this direction, providing a prerequisite for a one-dimensional spin transistor and yielding an extra degree of freedom in spin-orbit-interaction-based spintronics. We mentioned above that Fermi nesting takes place between

surface states with the same spin polarization. Strictly speaking, nesting occurs if the (absolute) $+k$ states are projected onto $-k$ states by a reciprocal lattice vector. Consequently, for Rashba-split surface states the nesting condition can be maintained only if both helicities get nested simultaneously, i.e., $k_{\uparrow(l)} \rightarrow -k_{\uparrow(l)}$, suggesting electronic correlation between Rashba states with time-reversal symmetry.

The Rashba splitting in the Pb/Si(557) system was found to be as large as 0.2 \AA^{-1} . Even by using moderate effective masses (e.g., 0.4 electron masses determined with electron energy loss spectroscopy [25]), this results in a Rashba parameter of 1.9 eV \AA , which is close to the largest value reported in literature for Bi/Ag(111) [26] or for metallic monolayer structures on semiconducting surfaces [27] and which is a factor of 50 larger than what was reported for Pb quantum well states on Si(111) [28].

As described by Bihlmayer *et al.* [9] and later expanded by Nagano *et al.* [8], the magnitude of the Rashba parameter depends on the wave function distribution around the atom core. Within this model, the main contributions to the spin splitting are the Z of the material [7], the orbital mixing, and the atomic corrugation [10]. The high Z of Pb alone can not explain the observed magnitude, as is clear from a comparison to the densely packed Pb monolayer on Ge(111) where $\alpha_R = 0.24 \text{ eV \AA}$ was found [29]. We are therefore left to conclude that the charge distribution is strongly altered by the wires and differs from the isotropic 2D case.

So far, electron-electron interaction in and between the wires has been neglected, thus demanding nesting between bands of the same spin helicity. Within a 1D Hubbard model with small on-site energies U , it has been shown that the actual ground state is a SDW [1]. Assuming a dynamic antiferromagnetic ordering of adjacent Pb wires, i.e., that the reciprocal lattice vector is $g' = g/2 = \pi/d$ rather than g as in the former CDW discussion, simultaneous transitions of $k_{\uparrow(l)} \rightarrow -k_{\uparrow(l)} = k_{\uparrow(l)} - g'$ are expected, and the superposition of left- and right-polarized SDW results in the formation of linearly polarized SDW with bidirectionally gapped surface states, similarly to the antiferromagnetism in Cr as discussed by Overhauser [18].

In summary, the spin texture of the surface states of Pb wires grown on Si(557) has been analyzed. The mutual relation between the (223) facet structure and the band filling factors results in Fermi nesting along the $[11\bar{2}]$ direction; i.e., the system is electrically insulating at low temperatures in this direction. The SOC giving rise to Rashba surface states in this system is such that the spin texture close to the FS is alternating and equidistant in momentum space. A deep theoretical understanding of this extraordinary large Rashba parameter in this strongly anisotropic system is nonexistent at the moment. Spin-polarized STM would be helpful in order to correlate the location of these states with the symmetry of the

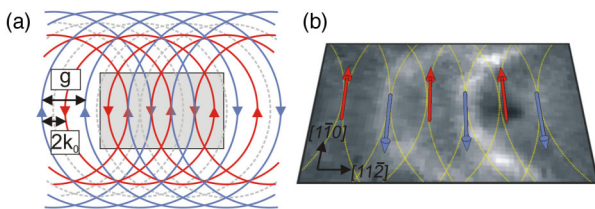


FIG. 5 (color online). (a) Schematic of intersecting Rashba-split Fermi circles (solid circles) under conservation of nesting between spin-polarized states along the $[11\bar{2}]$ direction. The dashed circles represent the FS without SOC. The phase space of the shaded (gray) rectangle is shown in (b). For the sake of simplicity, the flattening of the FS due to nesting is not considered. (b) Measured Fermi surface. The dotted (yellow) segments represent the spin-polarized surface states in (a). The vectors show the resulting in-plane spin polarization for different surface bands along the $[11\bar{2}]$ direction.

wires and to allow us to deduce a certain edge topology in this system.

Financial support by the Deutsche Forschungsgemeinschaft and the Swiss National Science Foundation is gratefully acknowledged.

*tegenkamp@fkp.uni-hannover.de

- [1] G. Grüner, *Density Waves in Solids* (Addison-Wesley, Reading, MA, 1994).
- [2] C. Blumenstein, J. Schäfer, S. Mietke, S. Meyer, A. Dollinger, M. Lochner, X.Y. Cui, L. Patthey, R. Matzdorf, and R. Claessen, *Nat. Phys.* **7**, 776 (2011).
- [3] H. Weiering, *Nat. Phys.* **7**, 744 (2011).
- [4] P.C. Snijders and H.H. Weiering, *Rev. Mod. Phys.* **82**, 307 (2010).
- [5] J.H. Dil, *J. Phys. Condens. Matter* **21**, 403001 (2009).
- [6] S.C. Erwin and F.J. Himpsel, *Nat. Commun.* **58**, 1056 (2010).
- [7] L. Petersen and P. Hedegård, *Surf. Sci.* **459**, 49 (2000).
- [8] M. Nagano, A. Kodama, T. Shishidou, and T. Oguchi, *J. Phys. Condens. Matter* **21**, 064239 (2009).
- [9] G. Bihlmayer, Y.M. Koroteev, P.M. Echenique, E.V. Chulkov, and S. Blügel, *Surf. Sci.* **600**, 3888 (2006).
- [10] I. Gierz, B. Stadtmüller, J. Vuorinen, M. Lindroos, F. Meier, J.H. Dil, K. Kern, and C.R. Ast, *Phys. Rev. B* **81**, 245430 (2010).
- [11] J.N. Crain, A. Kirakosian, K.N. Altmann, C. Bromberger, S.C. Erwin, J.L. McChesney, J.L. Lin, and F.J. Himpsel, *Phys. Rev. Lett.* **90**, 176805 (2003).
- [12] C. Tegenkamp, Z. Kallassy, H. Pfnür, H.-L. Günter, V. Zielasek, and M. Henzler, *Phys. Rev. Lett.* **95**, 176804 (2005).
- [13] C. Tegenkamp, T. Ohta, J.L. McChesney, H. Dil, E. Rotenberg, H. Pfnür, and K. Horn, *Phys. Rev. Lett.* **100**, 076802 (2008).
- [14] I. Barke, Fan Zheng, T.K. Rügheimer, and F.J. Himpsel, *Phys. Rev. Lett.* **97**, 226405 (2006).
- [15] T. Okuda, K. Miyamaoto, Y. Takeichi, H. Miyahara, M. Ogawa, A. Harasawa, A. Kimura, I. Matsuda, A. Kakizaki, T. Shishidou, and T. Oguchi, *Phys. Rev. B* **82**, 161410 (2010).
- [16] J. Lobo-Checa, F. Meier, J.H. Dil, T. Okuda, M. Corso, V.N. Petrov, M. Hengsberger, L. Patthey, and J. Osterwalder, *Phys. Rev. Lett.* **104**, 187602 (2010).
- [17] D. Lükermann, M. Gauch, M. Czubanowski, H. Pfnür, and C. Tegenkamp, *Phys. Rev. B* **81**, 125429 (2010).
- [18] A.W. Overhauser, *Phys. Rev.* **128**, 1437 (1962).
- [19] M. Hoesch, T. Greber, V.N. Petrov, M. Muntwiler, M. Hengsberger, W. Auwärter, and J. Osterwalder, *J. Electron Spectrosc. Relat. Phenom.* **124**, 263 (2002).
- [20] M. Czubanowski, A. Schuster, S. Akbari, H. Pfnür, and C. Tegenkamp, *New J. Phys.* **9**, 338 (2007).
- [21] C. Tegenkamp and H. Pfnür, *Surf. Sci.* **601**, 2641 (2007).
- [22] K.S. Kim, H. Morikawa, W.H. Choi, and H.W. Yeom, *Phys. Rev. Lett.* **99**, 196804 (2007).
- [23] F. Meier, H. Dil, J. Lobo-Checa, L. Patthey, and J. Osterwalder, *Phys. Rev. B* **77**, 165431 (2008).
- [24] F. Meier, J.H. Dil, and J. Osterwalder, *New J. Phys.* **11**, 125008 (2009).
- [25] T. Block, C. Tegenkamp, J. Baringhaus, H. Pfnür, and T. Inaoka, *Phys. Rev. B* **84**, 205402 (2011).
- [26] C.R. Ast, J. Henk, A. Ernst, L. Moreschini, M.C. Falub, D. Pacilé, P. Bruno, K. Kern, and M. Grioni, *Phys. Rev. Lett.* **98**, 186807 (2007).
- [27] P. Höpfner, J. Schäfer, A. Fleszar, J.H. Dil, B. Slomski, F. Meier, C. Loho, C. Blumenstein, L. Patthey, W. Hanke, and R. Claessen, *Phys. Rev. Lett.* **108**, 186801 (2012).
- [28] J.H. Dil, F. Meier, J. Lobo-Checa, L. Patthey, G. Bihlmayer, and J. Osterwalder, *Phys. Rev. Lett.* **101**, 266802 (2008).
- [29] K. Yaji, Y. Ohtsubo, S. Hatta, H. Okuyama, K. Miyamoto, T. Okuda, A. Kimura, H. Namatame, M. Taniguchi, and T. Aruga, *Nat. Commun.* **1**, 1 (2010).